JOURNAL

OF THE AMERICAN CHEMICAL SOCIETY

VOLUME 109, NUMBER 4 FEBRUARY 18, 1987

A Stepwise Mechanism for Gas-Phase Unimolecular Ion Decompositions. Isotope Effects in the Fragmentation of *tert*-Butoxide Anion

William Tumas, Robert F. Foster, Mark J. Pellerite, and John I. Brauman*

Contribution from the Chemistry Department, Stanford University, Stanford, California 93405.
Received March 24, 1986

Abstract: Infrared multiple photon (IRMP) photochemical activation of gas-phase ions trapped in an ion cyclotron resonance (ICR) spectrometer has been used to study the mechanism of a gas-phase negative ion unimolecular decomposition. Upon irradiation with a CO_2 laser (both high-power pulsed and low-power continuous wave (CW)), *tert*-butoxide anion, trapped in a pulsed ICR spectrometer, decomposes to yield acetone enolate anion and methane. The mechanism of this formal 1,2-elimination reaction was probed by measuring competitive hydrogen isotope effects (both primary and secondary) in the IR laser photolysis of 2-methyl-2-propoxide-*1,1,1-d*$_3$ (**1**) and 2-methyl-2-propoxide-*1,1,1,3,3,3-d*$_6$ (**2**) anions. Unusually large secondary isotope effects (pulsed laser, 1.9 for **1** and 1.7 for **2**; cw laser, 8 for **1**) and small primary isotope effects (pulsed laser, 1.6 for **1** and **2**; cw laser, 2.0 for **1**) were observed. These isotope effects, particularly the large difference in energy dependence of the primary and secondary effects, are consistent only with a stepwise mechanism involving initial bond cleavage to an intermediate ion–molecule complex followed by a hydrogen transfer within the intermediate complex. The observed secondary isotope effects have been modelled by using statistical reaction rate (RRKM) theory. The implications of this study for several previously reported unimolecular ion decompositions are also discussed.

Advances in ion generation and trapping techniques as well as ion detection methods have stimulated interest in understanding the dynamics and mechanisms of gas-phase ion reactions.[1-3] The availability of such techniques has lead to rapid development in the field of negative ion mass spectrometry.[4] In spite of the increasing number of reports on negative ion chemistry, no clear mechanistic picture has emerged for even simple negative ion unimolecular decompositions.

Efforts in our laboratory have been directed toward the use of photochemical activation of gas-phase ions trapped in an ion cyclotron resonance (ICR) spectrometer to induce negative ion fragmentations and to investigate reaction mechanisms. In this paper,[5] we report the details of our investigations into the infrared multiple photon[6] (IRMP) photochemically induced unimolecular elimination of methane from *tert*-butoxide anion, which is a prototypical example of 1,2-elimination of a neutral fragment from a negative ion.[7] We present competitive intramolecular kinetic hydrogen isotope effect measurements (both primary and secondary)[8,9] which support a stepwise mechanism for methane elimination from *tert*-butoxide anion that involves initial cleavage to an intermediate ion–molecule complex.[10] The observed secondary isotope effects have been modelled by using statistical reaction rate theory (RRKM theory) and are consistent with initial cleavage of the carbon–methyl bond as the rate-determining step. The implications of these results are discussed for several unimolecular decompositions reported in the literature, particularly

(1) *Gas Phase Ion Chemistry*; Bowers, M. T., Ed.; Academic Press: New York, 1979.

(2) Nibbering, N. M. M. *Mass Spec. Rev.* **1984**, *3*, 445. Dannacher, J. *Org. Mass Spec.* **1984**, *19*, 253. *Gas Phase Ion Chemistry: Ions and Light*; Bowers, M. T., Ed.; Academic Press: New York, 1983.

(3) Howe, I.; Williams, D. H.; Bowen, R. D. *Mass Spectrometry: Principles and Applications*; McGraw-Hill: New York, 1981. McLafferty, F. W.; *Interpretation of Mass Spectra*; University Science Books: 1980. *Current Topics in Mass Spectrometry and Chemical Kinetics*; Beynon, J. H., McClashan, M. L., Eds.; Heyden: London, 1982. Holmes, J. L. In *Isotopes in Organic Chemistry*; Buncel, E., Lee, C. C., Eds.; Elsevier: Amsterdam, 1975.

(4) Bowie, J. H. *Mass Spec. Rev.* **1984**, *3*, 161. Budzikiewicz, H. *Angew. Chem., Int. Ed. Engl.* **1981**, *20*, 624. Dougherty, R. C. *Anal. Chem.* **1981**, *53*, 625.

(5) A preliminary report of this work has appeared: Tumas, W.; Foster, R. F.; Pellerite, M. J.; Brauman, J. I. *J. Am. Chem. Soc.* **1983**, *105*, 7464.

(6) Reviews on IRMP photochemistry: Golden, D. M.; Rossi, M. J.; Baldwin, A. C.; Barker, J. R. *Acc. Chem. Res.* **1981**, *14*, 56. Schultz, P. A.; Sudbo, A. S.; Kranovich, D. J.; Kwok, H. S.; Shen, Y. R.; Lee, Y. T. *Ann. Rev. Phys. Chem.* **1979**, *30*, 379. Thorne, L. R.; Wight, C. A.; Beauchamp, J. L. In *Ion Cyclotron Resonance Spectrometry II*; Hartmann, H., Wanczek, K. P., Eds.; Springer-Verlag: Berlin, 1982; Vol. 31.

(7) Melander, L.; Saunders, W. H. *Reactions of Isotopic Molecules*; Wiley: New York, 1980.

(8) Derrick, P. J. *Mass Spec. Rev.* **1983**, *2*, 285.

(9) Elimination of alkanes and/or molecular hydrogen from alkoxide anions has been reported in several studies.[9,10] To date, however, there have been few studies which have provided much insight into how these simple negative ions dissociate: Boand, G.; Houriet, R.; Gaumann, T.; *Lect. Notes Chem.* **1982**, *31*, 195. Houriet, R.; Stahl, D.; Winkler, F. J. *Environ. Health Perspec.* **1980**, *36*, 63. Roy, T. A.; Field, F. H.; Lin, Y. Y.; Smith, L. L. *Anal. Chem.* **1979**, *51*, 272.

(10) For reviews on stepwise decompositions of positive ions, see: Bowen, R. D.; Williams, D. H. In de Mayo, P., Ed.; *Rearrangements in Ground and Excited States*; Academic Press: New York, 1980; Vol. 1. Williams, D. H. *Acc. Chem. Res.* **1977**, *10*, 280. Morton, T. H. *Tetrahedron* **1982**, *38*, 3195.

0002-7863/87/1509-0961$01.50/0

those involving apparent four-center 1,2-eliminations of neutral fragments.

Experimental Section

Materials. Nitrogen trifluoride (Ozark Mahoning Company), *tert*-butyl peroxide (MCB), acetone-d_6 (MSD Isotopes, 99.7% atom D), and iodomethane-d_3 (Aldrich, 99 % atom D) were obtained commercially and were used without further purification. Prior to use, *tert*-butyl alcohol was distilled under nitrogen from sodium metal. Dimethyl peroxide was prepared by the reaction of basic hydrogen peroxide with dimethyl sulfate following the method of Hanst and Calvert.[11] The gaseous product was collected in a trap at −78 °C and then dried by bulb-to-bulb distillation from activated 4-Å molecular sieves at 0 °C on a vacuum line.

Deuteriated *tert*-Butyl Alcohols. 2-Methyl-2-propanol-*1,1,1*-d_3 was prepared[12] by the addition of trideuteriomethylmagnesium iodide, generated from iodomethane-d_3 and magnesium turnings in ether, to acetone followed by hydrolysis with saturated aqueous ammonium chloride. After separation, numerous extractions of the aqueous layer with ether, and drying over anhydrous sodium sulfate, the alcohol was isolated by fractional distillation under an atmosphere of nitrogen (bp 82–84 °C). The fractions of high purity (>99%) were used in the ICR experiments. The d_6 analogue, 2-methyl-2-propanol-*1,1,1,3,3,3*-d_6, was synthesized in an analogous manner from methylmagnesium bromide (Aldrich) and perdeuteriated acetone (Aldrich). NMR and IR spectra were consistent with those in the literature. The isotopic purity of the alcohols was analyzed by ICR negative ion studies by using methoxide anion as a base for proton abstraction. No isotopic impurities could be detected (<2–3%); only one peak which corresponded to the (M-1) ion appeared in the negative ion mass spectrum of each alcohol.

Trimethylsilyl Ethers. The corresponding trimethylsilyl ethers of *tert*-butyl alcohol and 2-methyl-2-propanol-*1,1,1*-d_3 were synthesized by two different methods. In the first procedure, freshly distilled (from CaH_2) chlorotrimethylsilane (Aldrich; 1.1 equiv) was added to a pentane solution of the alcohol (1.0 equiv) and pyridine (1.1 equiv). After having been stirred at room temperature for 2 days, the reaction mixture was suction filtered to remove the voluminous white pyridine·HCl precipitate, and then the pentane was removed by distillation. The desired silyl ether was isolated by preparative gas chromatography (GC) of the residual oil (Hewlett-Packard 5790 equipped with a TC detector; 10% SE30 on Chrom WHP 80/100 mesh column (Alltech) at 70 °C). The second method, which was found to be more satisfactory, simply involved heating equimolar amounts of the neat alcohol and (trimethylsilyl)acetamide (Petrarch) at 80 °C for 24 h. The pure silyl ether was isolated by preparative GC of the resulting supernatant liquid (the byproduct acetamide precipitated).[13] The unlabeled silyl ether was characterized by gas chromatography (GC) and NMR and IR spectroscopy as well as its negative ion–molecule chemistry. The deuteriated species could then be characterized by GC and negative ion ICR studies.

The trimethylsilyl ethers were found to be quite stable with respect to hydrolysis in the ICR foreline. Hydrolysis could be detected in the negative ion chemical ionization mass spectrum (by using fluoride ion) as an appearance of a peak at $m/e = 89$ corresponding to deprotonated Me_3SiOH. If such evidence for hydrolysis was observed, a new sample of the silyl ether was used in another foreline.

Ion Generation. Primary negative ions were generated by the dissociative electron capture of appropriate precursors (at pressures of (1–5) × 10^{-7} torr): F^- from NF_3 (2–3 V electron energy) MeO^- from MeOOMe (2.5–3.5 V electron energy). *tert*-Butoxide anion was generated by deprotonation of *tert*-butyl alcohol with methoxide anion. The deuteriated alkoxide anions were prepared in an analogous manner from the deuteriated alcohols for most of the experiments. For the experiments involving CW CO_2 laser photolysis, the alkoxide anions were generated by the reaction of fluoride ion with the corresponding trimethylsilyl ethers. All compounds were degassed by several freeze–pump–thaw cycles on the ICR foreline before use.

Instrumentation. All experiments were performed on a pulsed ion cyclotron resonance spectrometer employing a trapped-ion analyzer cell modified for infrared multiple photon photochemical experiments as described previously.[14] The CO_2 lasers employed in this work, both of which are grating tuned, consisted of a commercial pulsed TEA laser (Lumonics TEA-103-2) and a CW laser constructed in our laboratory.

(11) Hanst, P. L.; Calvert, J. G. *J. Phys. Chem.* **1959**, *63*, 104.
(12) Wei, I. Y. *J. Labelled Compd.* **1974**, *10*, 355.
(13) For both methods it was essential to use preparatory gas chromatography for effective separation of the desired product from unreacted reagents and hexamethyldisiloxane which appeared as a significant side product.
(14) Jasinski, J. M.; Rosenfeld, R. N.; Meyer, F. K.; Brauman, J. I. *J. Am. Chem. Soc.* **1982**, *104*, 652.

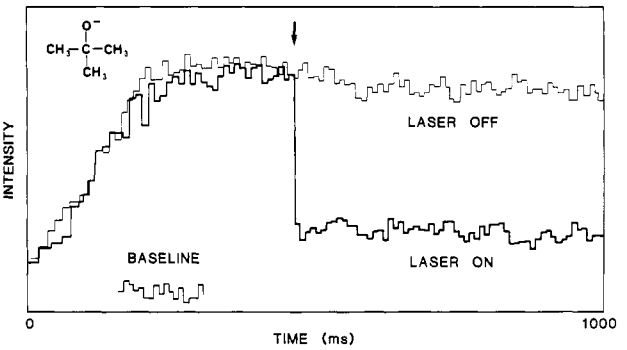

Figure 1. Time dependence of the *tert*-butoxide anion signal intensity in the presence and absence of pulsed laser irradiation. The arrow indicates the time in the duty cycle at which the laser is triggered.

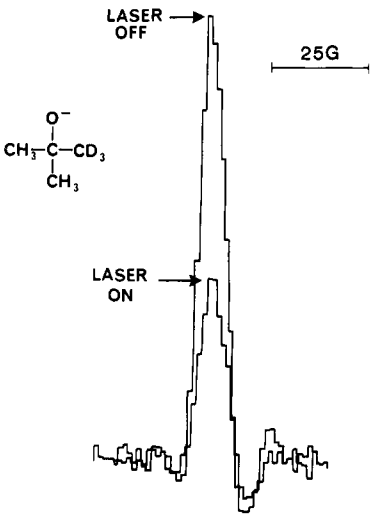

Figure 2. Unaveraged mass scan (magnetic field sweep) of 2-methyl-2-propoxide-*1,1,1*-d_3 without (upper trace) and with (lower trace) pulsed CO_2 laser irradiation.

Signal Averaging. In order to improve the signal/noise ratio in the photochemical experiments, extensive signal averaging was done by using a microcomputer. For large signals, the peak maxima were located from a single mass scan (see, for example, Figure 2). After establishing that there were no resonance frequency shifts upon irradiation, signal averaging was accomplished by adjusting the detector frequency to the peak maximum and measuring the signal intensity in the presence and absence of laser irradiation with all pulses fixed in time. This procedure was used to study all reactant ions as well as the product ion from unlabeled *tert*-butoxide anion. In the isotope effect determinations, however, several deuteriated photoproducts were formed from each reactant alkoxide ion; therefore, the signals were considerably smaller. It was much more difficult to assign clearly the peak maximum for each product ion from a single mass (frequency) scan, so a more elaborate method was used for signal averaging in these experiments. After the approximate resonant frequencies were determined, the microcomputer was used to accumulate data for a series of frequencies that bracketed the maximum of each signal. Typically 10–20 closely spaced frequencies for each ion signal were studied. The product ions were repetitively scanned about their maxima in this manner with and without laser irradiation. Typically 10–50 points were averaged for each frequency. The data were collected in groups of five points. Those groups for which the laser misfired one or more times were rejected and recollected. It was found that this type of signal averaging significantly increased the signal/noise ratio and permitted clear assignment of the peak maximum for each photoproduct ion (see, for example, Figure 3).

Results

***tert*-Butoxide Anion.** The *tert*-butoxide anion was generated by deprotonation of *tert*-butyl alcohol (ca. 10^{-6} torr) with methoxide ion (eq 2). The reaction went to completion within 100–150 ms. Upon irradiation with the unfocused output of a pulsed CO_2

$$CH_3OOCH_3 \rightarrow CH_3O^- + CH_3O^\bullet \quad (1)$$

$$CH_3O^- + t\text{-BuOH} \rightarrow t\text{-BuO}^- + CH_3OH \quad (2)$$

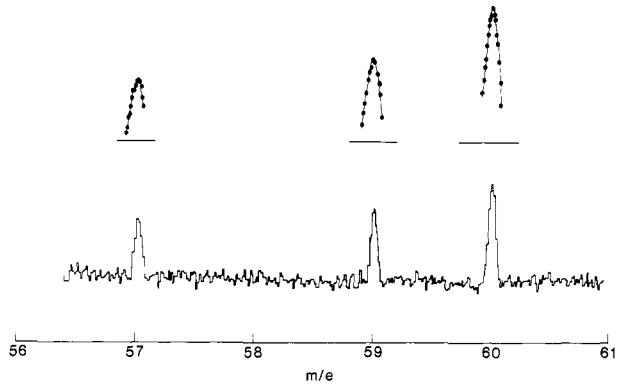

Figure 3. Unaveraged (lower trace) and averaged (upper trace) mass scan (frequency scan) of acetone enolate anions produced by pulsed CO_2 laser photolysis of 2-methyl-2-propoxide-*1,1,1-d*$_3$ anion.

laser, *tert*-butoxide ion undergoes IRMP dissociation resulting in the elimination of methane and the production of acetone enolate ion (eq 3). Decomposition could be effected with lines from both branches of the laser but maximized at $R(16)/10.6\mu$ (973 cm^{-1}). The extent of decomposition was not noticeably dependent on the pressure (5×10^{-7} to 1×10^{-5} torr) nor on the delay time between the grid and laser pulses for times up to 1 s. The amount of acetone enolate produced was equal to the amount of alkoxide decomposed. No other ionic products were detected. Vibrationally induced electron detachment[15] does not occur as verified by experiments designed to trap photoelectrons as chloride ion by using CCl_4. No photoincrease in the chloride ion signal was observed. Double resonance ejection[16] of the *tert*-butoxide ion prior to the laser pulse confirmed that the reaction occurs as shown (eq 3). The neutral product methane is inferred on the

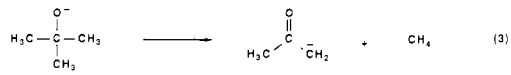

basis of mass balance and thermochemical considerations. As shown by the time dependence of the ion intensity (Figure 1), the alkoxide ion undergoes fragmentation on a submillisecond (unimolecular and collisionless) timescale. Furthermore, since the signal does not recover after the laser pulse, the alkoxide anion is not regenerated by any ion–molecule reactions. A corresponding increase in the intensity of the photoproduct acetone enolate which persists for the remainder of the duty cycle was also observed.

For the experiments involving irradiation with a continuous-wave CO_2 laser, *tert*-butoxide ion was generated by the reaction of fluoride ion with the trimethylsilyl ether of the alcohol[17] (eq 5). The results for the CW laser photolysis were similar to those

$$NF_3 \rightarrow F^- + NF_2 \quad (4)$$

$$F^- + t\text{-BuOSiMe}_3 \rightarrow t\text{-BuO}^- + Me_3SiF \quad (5)$$

obtained by using the pulsed laser. At similar fluences, the extent of decomposition was comparable for both lasers, indicating that the dissociation yield, which is fluence (energy per unit area) dependent, is insensitive to changes in laser intensity (power per unit area) of greater than 10^5.

Deuteriated Alkoxide Ions. The infrared photochemistry of 2-methyl-2-propoxide-*1,1,1-d*$_3$, **1**, and 2-methyl-2-propoxide-*1,1,1,3,3,3-d*$_6$, **2**, was investigated in an effort to measure competitive hydrogen isotope effects. For most of the pulsed laser experiments, these ions were generated from deprotonation of the corresponding alcohol with methoxide ion (analogous to the reaction in eq 2). Pulsed CO_2 laser irradiation of the d_3 alkoxide

Scheme I

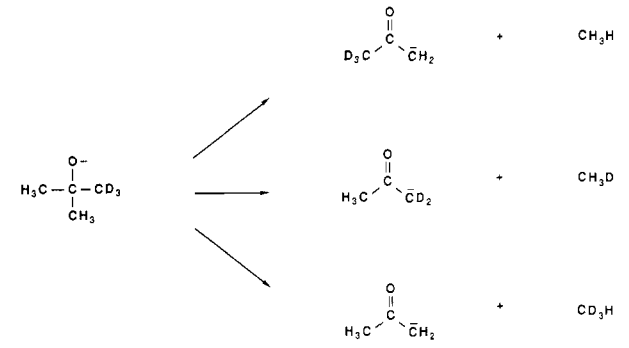

Scheme II

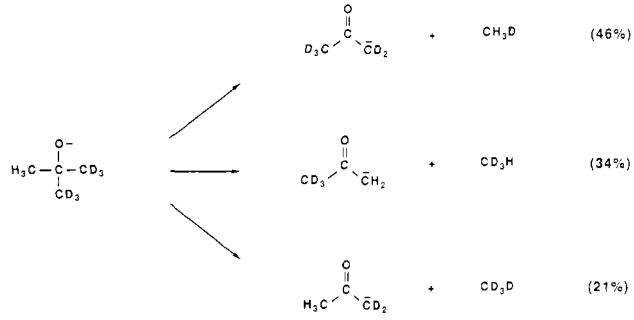

Table I. Percent Yields of Product Acetone Enolate Anions from CO_2 Laser Photolysis of 2-Methyl-2-propoxide-*1,1,1-d*$_3$ Anion (**1**)

laser	$CH_3\overset{O}{\overset{\|}{C}}CH_2^-$	$CH_3\overset{O}{\overset{\|}{C}}CD_2^-$	$CD_3\overset{O}{\overset{\|}{C}}CH_2^-$
pulsed	21 ± 2	31 ± 3	48 ± 3
CW	6 ± 2	32 ± 3	63 ± 3

ion **1** resulted in the production, in unequal amounts, of three isotopically substituted acetone enolate ions, d_0 (m/e = 57), d_2 (m = 59), and d_3 (m/e = 60), which arise from elimination of CD_3H, CH_3D, and CH_4, respectively (Scheme I). The sum of the intensities of the product ions was equal to the amount of the alkoxide decomposed. A typical unaveraged mass spectrum of the photoproducts along with the averaged scans through the maxima of the ion signals is shown in Figure 3. The relative yields of the isotopically distinct enolate ions are depicted in Table I. In order to maximize the extent of decomposition and hence maximize the signal intensity of the product enolate ions, all of the isotope effect determinations were carried out by using the highest possible laser fluences (2–3 J cm^{-2}). The dissociation yield maximized at $R(18)/10.6\mu$ (975 cm^{-1}). It was essential to detect the enolate ions immediately (5–25 ms) after the laser pulse, because the deuteriated enolate ions undergo hydrogen–deuterium exchange with the neutral alcohol.[18] If the ions were detected later in the duty cycle, the intensity of the d_3 and then the d_2 enolate was found to decrease with a corresponding increase in the d_0 enolate and the appearance of another ion at m/e = 58 corresponding to d_1 acetone enolate anion.

The pulsed laser-induced decomposition of the d_6 alkoxide **2** maximized at $R(32)/9.6\mu$ (1086 cm^{-1}) and resulted in the elimination of CD_4, CD_3H, and CH_3D; the d_2 (m/e = 59), d_3 (m/e = 60), and d_5 (m/e = 62) acetone enolate ions were formed, respectively. The product distribution, presented below, was found to be similar to the analogous distribution for **1** (see Scheme II).

In order to investigate the intensity dependence of the branching ratios (isotope effects), the CW CO_2 laser-induced decomposition of **1** was also studied. For these experiments, the alkoxide ion **1** was generated in the absence of any alcohol by reacting the corresponding trimethylsilyl ether with fluoride ion. This method

(15) Meyer, F. K.; Jasinski, J. M.; Rosenfeld, R. N.; Brauman, J. I. *J. Am. Chem. Soc.* **1982**, *104*, 663.
(16) Anders, L. R.; Beauchamp, J. L.; Dunbar, R. C.; Baldeschwieler, J. D. *J. Chem. Phys.* **1978**, *45*, 111.
(17) DePuy, C. H.; Bierbaum, V. M.; Flippin, L. A.; Grabowski, J. J.; King, G. K.; Schmitt, R. J.; Sullivan, S. A. *J. Am. Chem. Soc.* **1980**, *102*, 5012.

Table II. *tert*-Butoxide Anion Isotope Effects

alkoxide anion	laser	primary isotope effect	secondary isotope effect (concerted)	secondary isotope effect (stepwise)
1	pulsed	1.6	2.3	1.9
2	pulsed	1.6	2.1	1.7
1	CW	2.0	10	8

for ion generation was necessary since these experiments involve irradiating the alkoxide ions for several hundred ms with the CW CO_2 laser. During this time, the deuteriated product enolate ions would undergo H/D exchange[18] with any alcohol present in the ICR cell, and the relative ion abundances detected after the irradiation period would not reflect the true photochemical product distribution. When reaction 6 was used as the source of **1**, the intensities of the product ions were independent of time after the laser irradiation period. Furthermore, we were able to demonstrate in a separate set of experiments that the enolate ions themselves do not undergo IRMP-induced decomposition upon CW laser irradiation (unfocused). Thus, the relative abundances of the enolate ions measured after irradiation correspond to the true primary photochemical product distribution. While the overall dissociation yield of **1** was similar for both pulsed and CW irradiation and the nature of the photoproducts was identical, the relative abundances of the product acetone enolate ions were markedly different. In particular, very little acetone enolate-d_0 (the result of CD_3H elimination) was produced in the CW laser experiments. The results of the CW laser photolysis are displayed in Table I.

Calculation of Isotope Effects. The production of unequal amounts of isotopically distinct acetone enolate ions in the IR laser photolysis of **1** and **2** is a consequence of intramolecular kinetic hydrogen isotope effects. It is possible to calculate both primary and secondary isotope effects from the measured abundances, $[CX_3L]$,[19] of the product enolate ions. The nature of the correction for statistical factors and thus the method for extracting the isotope effects from the observed product distribution actually depends on the operative reaction mechanism (i.e., requires prior knowledge or assumption of a mechanism). Although the exact values of the isotope effects depend on the type of correction applied (for details see Appendix 1), the magnitude of these isotope effects for the mechanisms under consideration are, in fact, similar enough that it is not necessary to resolve this issue in order to draw mechanistic conclusions. For the sake of completeness we have included the calculated isotope effects for both a concerted and a stepwise mechanism in Table II.

Kinetic isotope effects can be calculated in a straightforward manner for any single-step (concerted) reaction pathway, since they are equivalent to the appropriate relative enolate ion intensities. For example, the product ratio $[CH_3H]/[CH_3D]$ from **1** corresponds to a primary isotope effect.[20] Similarly the primary isotope effect is the ratio $[CD_3H]/[CD_3D]$ from **2**. A primary effect of 1.6 is calculated for the pulsed laser-induced decomposition of both **1** and **2**. For the CW laser photolysis of **1**, a value of 2.0 is obtained (Table II). A secondary isotope effect can be calculated from the relative amounts of CH_3H and CD_3H elimination from **1** and from the ratio $[CH_3D]/[CD_3D]$ for **2** (values are listed in Table II). For a stepwise mechanism with more than one branching point, the isotope effects must be calculated differently because the statistical factors can appear in different steps. The values obtained assuming the stepwise mechanism depicted in eq 8 are listed in Table II also. Since the primary effect is the same for either mechanism under consideration (Appendix 1), only one entry is made for this isotope effect in Table II.

Discussion

Two possible mechanisms for the IRMP-induced fragmentation of *tert*-butoxide anion are shown below.[22] One is a simple concerted four-centered elimination of methane (eq 7). The other is a stepwise pathway involving an initial cleavage (either heterolytic or homolytic) to form an intermediate ion–molecule complex, I, and a subsequent proton (or hydrogen atom) transfer within the complex[21] (eq 8).

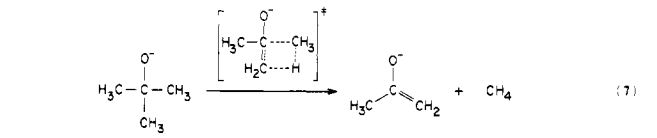

(7)

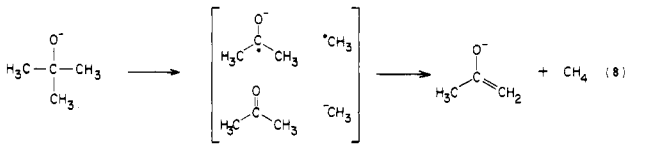

(8)

I

The two mechanistic possibilities cannot be distinguished on the basis of energetics because it is not possible to estimate the critical energy for the concerted pathway (eq 7). The unimolecular elimination of HX from alkyl halides, a good example of a concerted four-center elimination, has been extensively studied by a variety of activation methods.[23] Activation energies for these reactions range from 45 to 60 kcal/mol. Elimination of methane from neutral compounds such as acetone, isobutane, *tert*-butyl amine, and *tert*-butyl alcohol have been reported to have activation energies[24] in excess of 60–65 kcal/mol. These reactions may, however, involve radical chain mechanisms and surface-catalyzed processes. There is an extensive literature on methane (and alkane) elimination from the gaseous radical cations of several hydrocarbons, alcohols, ethers, amines, and ketones;[25] in certain cases, the threshold energy has been determined from appearance energies. Since these reactions do not necessarily proceed through a concerted four-center mechanism (vide infra), these measurements may not be pertinent to the concerted pathway for *tert*-butoxide anion.

(18) DePuy, C. H.; Bierbaum, V. M. *Acc. Chem. Res.* **1981**, *14*, 146. Squires, R. R.; DePuy, C. H.; Bierbaum, V. M. *J. Am. Chem. Soc.* **1981**, *103*, 4256.

(19) $[CX_3L]$ denotes the abundance of the enolate ion resulting from CX_3L elimination (X, L = H, D).

(20) This so called primary effect also contains a contribution from a secondary isotope effect because the L atom in the eliminated CX_3L was originally bonded to an sp^3 hybridized carbon of a CL_3 group which becomes sp^2 hybridized in the CL_2 group of the product. Since this secondary effect cannot be separated from the presumably larger primary effect, we have labeled this composite isotope effect as a primary effect in an effort to distinguish it from the other more important and separable secondary effect listed in Table II.

(21) A third mechanistic possibility involves a hidden proton transfer from carbon to oxygen prior to any fragmentation reaction. The general problem of hidden proton transfers in unimolecular decompositions of gas-phase ions (including those from carbon to oxygen) has been addressed and explored by Schwarz. In as much as this type of mechanism would be expected to exhibit inverse secondary kinetic isotope effects which are not observed in our study, we rule out this mechanism for *tert*-butoxide anion. Schwarz, H. *Top. Curr. Chem.* **1981**, *97*, 2. Hemberger, P. H.; Kleingeld, J. C.; Levsen, K.; Mainzer, N.; Mandelbaum, A.; Nibbering, N. M. M.; Schwarz, H.; Weber, R.; Weisz, A.; Wesdemiotis, C. *J. Am. Chem. Soc.* **1980**, *102*, 3736.

(22) The elimination of methane from *tert*-butoxide anion is a thermoneutral reaction, as calculated from the known heats of formation of the reactant and products. Relevant heats of formation (in kcal/mol): *tert*-butoxide anion, −68.6; acetone enolate anion, −50.1; methyl anion, 32.5; acetone, −51.7; methane, −17.9. Taken from Bartmess, J. E.; McIver, R. T., Jr. In *Gas Phase Ion Chemistry*; Bowers, M. T., Ed.; Academic Press: New York, 1979. Benson, S. W. *Thermochemical Kinetics*; Wiley-Interscience: New York, 1976.

(23) Dees, K.; Setzer, D. W. *J. Chem. Phys.* **1968**, *49*, 1193. Maccoll, A. *Chem. Rev.* **1969**, *69*, 33. Maccoll, A.; Thomas, P. J. *Prog. Reac. Kinet.* **1967**, *4*, 119.

(24) Winkler, C. A.; Hinshelwood, C. *Proc. R. Soc. London, A* **1935**, *A149*, 340. Peard, M. G.; Stubbs, F. J.; Hinshelwood, C. *Proc. R. Soc. London, A* **1952**, *A214*, 330. Prichard, H. O.; Sowden, R. G.; Trotman-Dickenson, A. F. *J. Chem. Soc.* **1954**, 546. Tsang, W. J. *J. Chem. Phys.* **1964**, *40*, 1498.

(25) Recent review: Hudson, C. E.; McAdoo, D. J. *Int. J. Mass Spec. Ion Phys.* **1984**, *59*, 325.

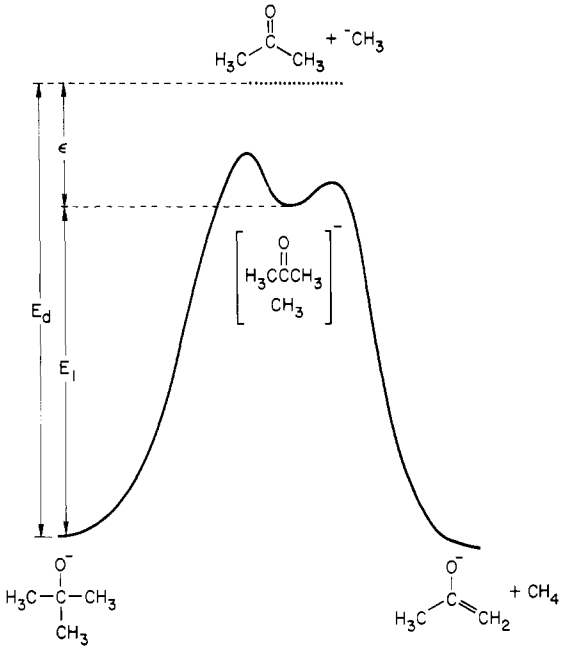

Figure 4. Schematic representation of the reaction coordinate for the stepwise mechanism for methane elimination from *tert*-butoxide anion. The energetics are described in the text.

Reasonable estimates of the energetics can be made for the stepwise mechanism. An energy profile of the reaction coordinate is illustrated in Figure 4. The endoergicity of the first step (formation of the intermediate ion–molecule complex, I), E_1, can be estimated from the energy required for cleavage to the free ion and molecule, E_d, and the ion–molecule interaction energy, ϵ: $E_1 = E_d - \epsilon$. Dissociation of *tert*-butoxide anion to separated methyl anion and acetone is endoergic by 49 kcal/mol. Because the electron affinities (EA's) of both methyl radical[26] and acetone[27] are very small, E_d for a homolytic cleavage (to methyl radical and acetone radical anion) would be approximately equal to that for the heterolytic cleavage. It is more difficult to evaluate the stabilization energy, ϵ, relative to dissociation of the intermediate ion–molecule complex. The binding energy of loose ion–molecule complexes such as I, which is mainly due to electrostatic factors such as ion–dipole and ion-induced dipole forces as well as other interactions such as hydrogen bonding, can be rather large. On the basis of the reported gas-phase ion studies of ion–molecule association equilibria, the stabilization of I for a heterolytic mechanism should probably be 10–15 kcal/mol.[28] In Figure 4, an activation barrier for the first step in excess of the thermodynamic barrier is shown. Although we have no direct experimental evidence for the size of this barrier, we believe that the barrier for the reverse reaction, addition of methyl anion to acetone, would not be very large based on several reported experimental and theoretical barriers for the addition of nucleophiles to carbonyls[29] and the large exothermicity involved here. Thus, we estimate the critical energy for the first step in the stepwise mechanism to be ca. 40–45 kcal/mol. The barrier for proton (or hydrogen atom) transfer within the complex, which constitutes the second step in this mechanism, would also be expected to be relatively low (a few kcal/mol), because this transfer is highly exothermic.

(26) The electron affinity of methyl radical has been determined to be 1.8 kcal/mol: Ellison, G. B.; Engelking, P. C.; Lineberger, W. C. *J. Am. Chem. Soc.* **1978**, *100*, 2556. These authors also assigned a value of 460 cm^{-1} for ν_2 in the anion based on a hot band in the laser photodetachment spectrum of methyl anion.

(27) Few data on the electron affinities of simple carbonyl compounds exist; however, the EA of these species, including acetone, is probably very small. Jordan, K. D. *Acc. Chem. Res.* **1978**, *12*, 36.

(28) Kebarle, P. *Ann. Rev. Phys. Chem.* **1977**, *28*, 445.

(29) For example: Asubiojo, O. I.; Brauman, J. I. *J. Am. Chem. Soc.* **1979**, *101*, 3715. Kovach, I. M.; Elrod, J. P.; Schowen, R. L. *J. Am. Chem. Soc.* **1980**, *102*, 7530.

Isotope Effects. Intramolecular kinetic isotope effects[30] represent the relative rates of competitive reactions of the same reactant and, therefore, depend only on the properties of the transition states of the isotopically distinct pathways. The only relevant properties of the reactant are those that determine the distribution of the total energy of the reacting species. Within the frameworks of statistical reaction rate theory (e.g., RRKM theory) and the Born–Oppenheimer approximation, intramolecular isotope effects arise solely from the interplay of differences in critical energies and densities of states.[30] Differences in critical energies (reaction thresholds) are caused by isotopically sensitive vibrations that change in the critical configuration or transition state (zero-point energy effects). Modification of the vibration frequencies and moments of inertia by isotopic substitution also results in differences in the sums of states for each transition state (entropic effects).

IRMP photochemistry involves activation into the rovibrational manifold of a molecular system by the sequential, incoherent absorption of infrared photons (ca. 3 kcal/mol each for CO_2 laser irradiation).[6] Since intramolecular energy randomization is generally much faster than both sequential activation (laser pumping rates) and the rates of most reactions, IRMP-induced reactions can be described by statistical reaction rate theory. Thus, the primary and secondary isotope effects observed in the IRMP-induced decomposition of *tert*-butoxide anion should be explainable entirely in terms of zero-point energy effects and state sum effects. At moderate energies the first effect would be expected to dominate.

The energy distribution of reacting molecules in an IRMP experiment can be far from thermal; therefore, the isotope effects do not represent ratios of thermal rate constants. The magnitude of these effects can be quite different from those typically encountered in solution or high-pressure gas-phase reactions which are characterized by a Boltzmann distribution at a well-defined temperature. The isotope effects in IRMP photochemically induced fragmentations correspond to ratios of microcanonical rate constants, $k(E)$, averaged over some nonthermal energy distribution $P(E)$.[30] In an IRMP experiment, the energy of the reacting species is determined by the laser pumping rate, k_p. Since the pumping rate from pulsed lasers[31] is generally greater than most reaction rates at threshold, it is quite likely that molecules or ions activated with such a laser decompose at energies somewhat above the critical energy. Conversely, the pumping rate for a CW laser is 5–6 orders of magnitude less than that for a pulsed laser. In this case, the pumping rate[32] is much less than the rate of most unimolecular decompositions even at threshold; hence, the reacting species must decompose very close to threshold. So, in addition to studying the magnitude of isotope effects, considerable information about their energy dependence can be obtained from studies employing both pulsed and CW lasers. Pulsed lasers permit access to an energy regime significantly above the reaction threshold energy, while CW lasers allow sampling of the isotope effects at or near the critical energy.

As discussed below, the magnitude and energy dependence of the primary and secondary isotope effects for the fragmentation of *tert*-butoxide anion (Table II) are consistent *only* with a stepwise mechanism (eq 8). The magnitudes of the isotope effects in the pulsed laser experiments, which we believe are more consistent with the stepwise pathway, do not in themselves provide enough evidence for any one particular mechanism. The key feature of this study is that the observed energy dependence of the primary and secondary isotope effects (i.e., the observed values for *both* pulsed and CW laser activation) does, however, establish the

(30) Forst, W. *Theory of Unimolecular Reactions*; Academic Press: New York, 1973. Robinson, P. J.; Holbrook, K. A. *Unimolecular* Reactions; Wiley: London, 1972.

(31) The pumping rate is given by the product of the cross section for photon absorption and the intensity of the incident laser irradiation. A typical cross section for absorption of an infrared photon is 10^{-19} cm^2. For a pulsed laser with a mean pulse intensity of ca. 10^{26} photons cm^{-2} s^{-1}, the pumping rate constant (from one level to the next) is calculated to be about 10^7 s^{-1}.

(32) At an intensity of 10 J cm^{-2} s^{-1}, the pumping rate is ca. 10^2 s^{-1}.

stepwise pathway by ruling out the concerted mechanism. The magnitude of the isotope effects will be addressed first, and then the energy dependence will be discussed.

The large secondary isotope effect (pulsed laser: 1.9 for **1** and 1.7 for **2**; CW laser: 8 for **1**; CH_3 elimination in preference to CD_3 elimination in CX_3L) requires a severe loosening of the eliminated methyl moiety in the transition state relative to the reactant ground state. If some or all of the frequencies of the isotopically sensitive vibrations of the methyl group decrease considerably upon formation of the transition state (critical configuration), then the critical energy for methane elimination involving a CH_3 group would be less than the elimination involving a CD_3 due to zero-point energy effects. A priori, it is difficult to predict the expected secondary isotope effect for the concerted four-center elimination. Intuitively, one might expect that the methyl group vibrations would not decrease considerably in the tight four-center transition state, so we would expect the secondary effect to be rather small for the concerted mechanism. The stepwise mechanism involves cleavage to a methyl radical or anion (in an ion–molecule complex) as the first rate-determining step. The transition state (and therefore its zero-point energy) would be expected to resemble closely the intermediate for such an endothermic reaction (Figure 4) especially if the barrier in excess of the thermodynamic barrier is not very large. All of the vibrational frequencies of methyl radical and its d_3 counterpart have been assigned either experimentally or theoretically.[33] The ν_2 umbrella mode is considerably weaker in the free radical than in a covalently bonded methyl group (607 vs. ca. 1360 cm^{-1} for CH_3 and 460 vs. ca. 1030 cm^{-1} for CD_3); frequencies of the other vibrations in methyl radical are similar to their counterparts in a bonded methyl moiety.[34] As discussed below, two other modes of the bonded methyl group are significantly weakened in the transition state and can be modeled as hindered rotors.

The small primary effect (pulsed laser: 1.6 for **1** and **2**; CW laser: 2.0 for **1**) indicates a small zero-point energy difference in the transition states for CX_3H and CX_3D elimination. These values are also consistent with a stepwise mechanism where the primary effect is manifested only in the second step involving a hydrogen atom or a proton transfer (within the ion–molecule complex). Although this step is probably not rate-determining, it is still possible to observe competitive isotope effects because this step is product-determining. Due to the large exothermicity of this step (ca. 40 kcal/mol), this hydrogen transfer reaction would proceed through a highly asymmetric transition state and thus should exhibit a small primary isotope effect.[7,36]

The small primary isotope effects are also consistent with a concerted mechanism in that this pathway involves a bent four-center transition state. For thermal systems, hydrogen transfer reactions that proceed through bent (nonlinear) transition states should exhibit small isotope effects (less than maximum effects).[7,36] The competitive primary isotope effects reported for thermally induced HX eliminations from alkyl halides[26] constitute a good example of this phenomenon.

While the magnitude of the isotope effects suggests a stepwise process, the energy dependence of these effects (obtained by comparing the results from CW and pulsed laser experiments) provides the most convincing evidence against a concerted mechanism and in support of a multistep reaction mechanism. The energy dependence (i.e., laser intensity dependence) of the primary and secondary effects are substantially different. The secondary effect is markedly dependent on the internal energy of the system, whereas the primary effect is relatively insensitive. The model calculations described below reveal that abnormally large secondary isotope effects in CW laser photolysis experiments arise because the system reacts very close to threshold. Under such conditions the zero-point energy differences of the isotopically distinct reaction channels are comparable to the excess internal energy of the reacting ions, so the branching ratios (isotope effects) are sensitive to even small differences in the critical energies. The result is that large isotope effects are observed. This situation is analogous to the reported large isotope effects in the decomposition of metastable positive ions.[8,40]

If a concerted mechanism were operative, then the respective zero-point energy differences giving rise to the secondary and primary isotope effects would have to be similar given that these isotope effects are similar for the pulsed laser-induced decomposition. The primary isotope effect should then also be abnormally large (i.e., exhibit threshold behavior) in the CW laser photolysis, contrary to experiment. The fact that we observe threshold behavior for one of the isotope effects (secondary) and not the other (primary) implies the existence of two transition states along the reaction coordinate. In other words, for the CW laser experiments, the system reacts at threshold for the step in which the secondary isotope effect arises but not at threshold for the step involving the primary isotope effect. The two effects *cannot* arise in the same transition state. The large amplification of the secondary effect upon changing from a high-power pulsed to a low-power CW laser reveals that this isotope effect arises from branching in a rate-limiting step. The primary isotope effect must occur in a subsequent step which, although product-determining, is kinetically insignificant. These conditions are consistent with the proposed multistep scheme (eq 8) if the barrier for the first step is larger than that for the second step (Figure 4). The large variation in the secondary isotope effect with internal energy would then be due to the step involving rate-determining cleavage of the carbon–methyl bond. Only slight differences would be expected for the primary effect for the rapid and highly exothermic hydrogen transfer in the second step because the internal energy of the system would be above the reaction barrier for this step for both pulsed and CW laser photolysis. In this case, we would not expect any unusually large threshold effects for the primary isotope effect in the CW laser photolysis.

Results of Model Calculations

In an effort to place the above interpretation on a more quantitative basis, we have modeled the secondary isotope effect and its energy dependence for the multistep mechanism by using RRKM theory.[30] In this section, we present the results of our model calculations[37] on the secondary isotope effect in the first step of the stepwise mechanism for the unimolecular decomposition of 2-methyl-2-propoxide-*1,1,1-d*$_3$ anion.[38] Specific details on these calculations including the transition state models and the input

(33) Tan, L. Y.; Winer, A. M.; Pimentel, G. C. *J. Chem. Phys.* **1972**, *57*, 4028. Snelson, A. *J. Phys. Chem.* **1970**, *74*, 537. Andrews, L.; Pimentel, G. C. *J. Chem. Phys.* **1967**, *47*, 3637. Jacox, M. E. *J. Mol. Spectrosc.* **1977**, *66*, 272.

(34) Although methyl anion appears to be pyramidal (ca. 20° deviation from planarity), experimental (ref 23) and theoretical (ref 35) studies imply that its vibrational frequencies are similar to those of methyl radical.

(35) Marynick, D. S.; Dixon, D. A. *Proc. Natl. Acad. Sci. U.S.A.* **1977**, *74*, 410. Poirier, R. A.; Daudel, R.; Mezey, P. G.; Csizmadia, I. G. *Int. J. Quantum Chem.* **1980**, *18*, 715.

(36) More O'Ferrall, R. A. In *Proton Transfer Reactions*; Caldin, E. F., Gold, V., Eds.; Chapman and Hall: London, 1975.

(37) Hase, W. L.; Bunker, D. L. *QCPE No. 234*, Indiana University.

(38) We have modelled the observed overall secondary isotope effect by calculating the secondary isotope effect for the first step involving cleavage of the carbon–methyl bond (i.e., $k_1^{CH_3}/k_1^{CD_3}$; where the k's are the microcanonical rate constants defined in Appendix 1. For a stepwise mechanism in general, an observed overall isotope effect does not necessarily correspond to the kinetic isotope effect for any one particular step (ref 7), especially if no one step is clearly rate-determining. For a two-step mechanism the observed isotope effects depend on the relative critical energies for the two transition states, the internal energy of the reacting species, and the zero point energy differences of the two transition states. If the first step is irreversible, i.e., rate-limiting, then the observed secondary isotope effect is identical with the secondary isotope effect for the first step. Although reversibility of the first step will generally lead to a significant deviation of the observed isotope effects from the isotope effect in the first step (ref 7), the deviation is nominal for reactions such as the unimolecular decomposition of *tert*-butoxide anion that involve highly endoergic bond cleavages to intermediates that are not in deep potential wells. The observed secondary isotope effect would vary between the kinetic isotope effect for the first step (completely irreversible) and the equilibrium isotope effect for the cleavage reaction (preequilibrium). For endoergic cleavage reactions the structure of the transition state for the bond cleavage and the intermediate are similar; therefore, the kinetic and equilibrium isotope effects for the first step are nearly equal (Appendix 1). The end result is that the observed secondary isotope effect is essentially determined by the transition state for the first step.

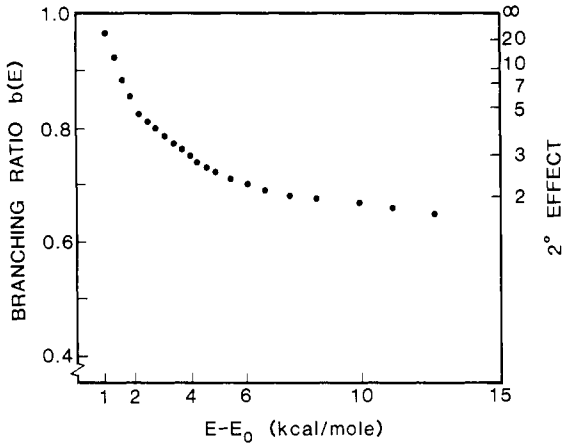

Figure 5. Results from the model calculations on the secondary isotope effects for the stepwise decomposition of 2-methyl-2-propoxide-*1,1,1-d*$_3$ anion (**1**). E_0 corresponds to the critical energy for the lower energy channel (CH_3 cleavage).

parameters are presented in Appendix 2.

The calculated secondary isotope effects for the stepwise mechanism, which monotonically decrease with increasing internal energy, are displayed graphically in Figure 5. To ascertain the sensitivity of these calculations to the input parameters, a number of calculations were done incorporating a range of critical energy differences between CH_3 and CD_3 cleavage (ΔE_0 ranging from 0.3 to 1.0 kcal/mol; CH_3 cleavage lower in energy) and model frequencies (100, 200, and 300 cm^{-1}) for the low-energy vibrations in the transition state that become internal rotations in the intermediate. As expected, the magnitude of the isotope effect is sensitive to the value of ΔE_0, especially at low excess internal energies. On the other hand, the shape of the curve in Figure 5 is not very sensitive to the input values for the modeled transition state frequencies. This is not surprising since the zero-point energy difference should be the major contributor to the isotope effect at moderate internal energies.

In addition to the secondary isotope effect calculations, we also calculated the absolute rate constants for cleavage of the carbon-methyl bond (i.e., the first step leading to the intermediate).[37] Reported frequencies for *tert*-butyl alcohol[39] were used to model the reactant *tert*-butoxide anion.

The experimentally observed secondary isotope effects[38] obtained from the product distribution in the IRMP experiments result from an averaging of the microcanonical rate constants over an energy distribution, $P(E)$.[30] Although a quantitative expression

$$k/k' = \frac{\int_{E_0}^{\infty} k(E)P(E)\,dE}{\int_{E'_0}^{\infty} k'(E)P(E)\,dE} \qquad (9)$$

for $P(E)$ cannot be formulated for our experiments, considerable insight into the origin of the energy dependence of the secondary effect can be obtained from qualitative considerations. The calculated isotope effects are in good agreement with the pulsed laser results. The mean pumping rate[31] for the pulsed CO_2 laser used in these experiments is estimated to be ca. 10^7 s^{-1}. The rate of the cleavage reaction ($k(E)$ for the first step) is greater than this pumping rate at excess internal energies corresponding to only a few infrared photons (6–12 kcal/mol). The ions must therefore be reacting in this energy regime, although the distribution could be rather broad. Around this energy, the calculated secondary isotope effects effectively model the observed effects.

The above calculations also help explain the unusually large secondary isotope effects for the CW laser-induced decomposition. Inspection of Figure 5 reveals that the secondary isotope effect can be very large at energies very close to the critical energies. In fact, if the internal energy of the system were between the critical energies of the two isotopically distinct channels, then an infinite isotope effect would result. The large secondary isotope effects in the CW laser experiments are simply a manifestation of the energy distribution of the reacting ions. Our qualitative predictions of the magnitude of the secondary isotope effect and its energy dependence for the stepwise mechanism are thus supported by the calculations, further substantiating a multistep scheme. The lack of such a large energy (intensity) dependence for the primary effect rules out the concerted mechanism in that it requires that the primary effect does not arise in the same transition state as the secondary effect (which is very large near threshold) but rather that it originates in a transition state with a lower critical energy than that of the overall reaction (defined by E_0 for the rate-determining step). Under the low-pressure experimental conditions where the collision rate is much slower than the rate of a unimolecular decomposition, the intermediate in the stepwise mechanism would contain an amount of excess internal energy determined by the barrier for the first step even when activated by a CW laser. If the barrier of the second step is lower, then the hydrogen transfer reaction (and thus the primary isotope effect) would always occur at energies above the critical energy for the second step, so no large primary isotope effect (i.e., threshold values) would be expected in the CW laser photolysis.

Mass Spectrometric Fragmentations[40,45]

Primary and secondary hydrogen isotope effects have been reported for metastable decompositions of alkane radical cations and related systems that involve the loss of an alkyl radical or the elimination of an alkane.[43] Large isotope effects have also been reported for alkane elimination from metastable ionized alcohols, ketones and amines. Hudson and McAdoo have recently concluded[29] from published isotope effects and energetic measurements that the elimination of alkanes from radical cations occurs in a stepwise manner through intermediate ion–radical complexes. There is now considerable precedent for the ion–molecule complexes as intermediates in a wide range of reactions of gaseous positive ions.[10,49] The present study, in conjunction with our model calculations, further substantiate the intervention of stepwise pathways in unimolecular ion decompositions.

Of particular relevance to the present study is the formal 1,2-elimination of methane from metastable 2-methylpropane radical cations to yield propene radical cations[44] (eq 10). Reported

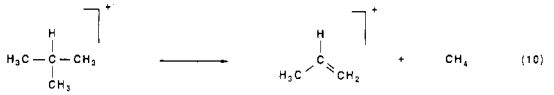

(10)

intramolecular kinetic isotope effects are similar to those for the CW laser-induced methane elimination of methane from *tert*-butoxide anion reported here. A large secondary effect of ca. 20 (CH_3D over CD_4 in the d_6 ion) and a small primary effect of 2.5 were taken as evidence that the reaction does not proceed via a concerted four-center mechanism for methane elimination.[44] These isotope effects were interpreted in terms of a nonclassical transition state involving a three-center bond analogous to the structure

(39) Korppi-Tommola, J. *Spect. Acta* **1978**, *34A*, 1077.

(40) Large intramolecular kinetic isotope effects (both primary and secondary) have been reported for metastable ion decompositions (ref 8, 41–44). The internal energy of metastable ions is generally distributed fairly narrowly just above the reaction threshold. So, analogous to the low power CW laser-induced ion decompositions, unusually large isotope effects are just a manifestation of the internal energy distribution of the reacting ions.

(41) Hills, L. P.; Vestal, M. L.; Futrell, J. H. *J. Chem. Phys.* **1971**, *54*, 3834. Ottinger, C. *Z. Naturforsch.* **1965**, *20*, 1232. Dibeler, V. H.; Rosenstock, H. M. *J. Chem. Phys.* **1963**, *39*, 1326. Lohle, U.; Ottinger, C. *J. Chem. Phys.* **1969**, *51*, 3097. Gordon, S. M.; Krige, G. J.; Reid, N. W. *Int. J. Mass Spec. Ion Proc.* **1974**, *14*, 109.

(42) Vestal, M.; Futrell, J. H. *J. Chem. Phys.* **1970**, *52*, 978. Donchi, K. F.; Brownlee, R. T. C.; Derrick, P. J. *Chem. Commun.* **1980**, 1061. Wolkoff, P.; Holmes, J. L. *J. Am. Chem. Soc.* **1978**, *100*, 7346.

(43) Holmes, J. L.; Burgers, P. C.; Yousuf, M.; Mollah, A.; Wolkoff, P. *J. Am. Chem. Soc.* **1982**, *104*, 2879. Holmes, J. L.; Burgers, P. C.; Mollah, Y. A. *Org. Mass Spec.* **1982**, *17*, 127. Hammerum, S.; Donchi, K. F.; Derrick, P. J. *Int. J. Mass Spec. Ion Phys.* **1983**, *47*, 347. Wolkoff, P.; Holmes, J. L. *J. Am. Chem. Soc.* **1978**, *100*, 7346.

(44) Mead, P. T.; Donchi, K. F.; Traeger, J. C.; Christie, J. R.; Derrick, P. J. *J. Am. Chem. Soc.* **1980**, *102*, 3364.

Scheme III

Stepwise Mechanism

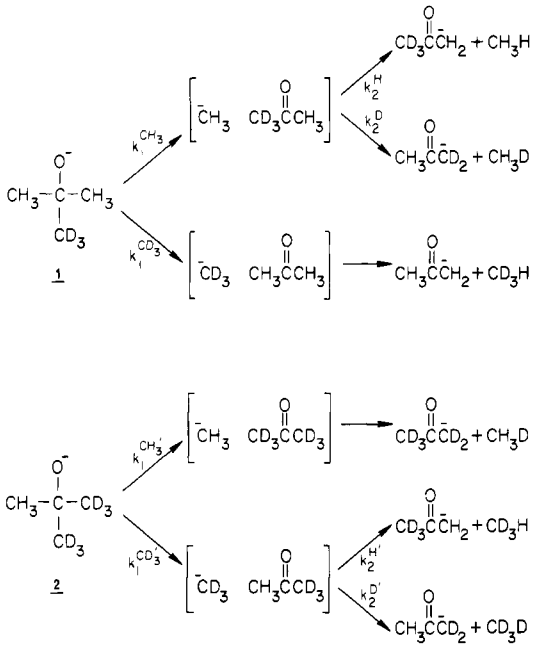

proposed for the reaction of 2-methylpropane with superacids. Our results suggest that these isotope effects are equally consistent with a stepwise mechanism involving initial cleavage to an intermediate complex consisting of isopropyl cation and methyl radical followed by a rapid hydrogen transfer to yield the ultimate products (eq 11).

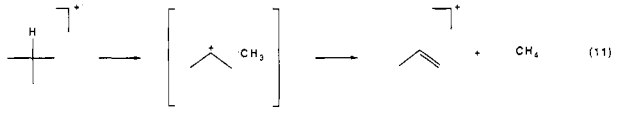

Conclusion

Competitive intramolecular kinetic isotope effects have been used to elucidate the mechanism of the IRMP-induced elimination of methane from *tert*-butoxide anion to produce acetone enolate ion. A large secondary isotope effect which is strongly dependent on laser intensity (and thus internal energy) and a small primary effect which is relatively insensitive to excess internal energy were observed. The magnitude and energy dependence of these isotope effects exclude a concerted four-center mechanism and are interpreted in terms of a stepwise mechanism involving initial cleavage to an intermediate ion–molecule complex followed by a hydrogen transfer reaction within the complex. Secondary isotope effects were modeled using RRKM theory. The isotope effects do not permit distinguishing between an initial heterolytic or homolytic cleavage (to yield an intermediate consisting of methyl anion and acetone or methyl radical and acetone radical anion, respectively), because the frequencies of the methyl moieties are very similar. Studies in our laboratory on other alkoxide ions, however, strongly suggest a heterolytic cleavage of the carbon–methyl bond in *tert*-butoxide anion.[50]

Table III

Transition State A: CD_3 Cleavage

Frequencies (cm^{-1})			
3018 (2)	2970	2963	
2944 (2)	2362 (2)	2153	
1731	1454	1435	
1426	1410	1364 (2)	1216
1025 (2)	891	877	
787	527	484	
461	385	200 (2)	
150 (2)	109	105	

Frequency Grouping

2976 (6) 2290 (3) 1419 (8) 1051 (4) 850 (3) 461 (4) 148 (6)

Moments of Inertia (amu-A^2): 6.0 (1-D, σ = 3)

Transition State B: CH_3 Cleavage

Frequencies (cm^{-1})		
3161 (2)	3044	3018
2968	2922	2265
2222	2141	1734
1447	1430	1398 (2)
1360	1224	1058
1035	1030	1003
999	781	764
740	607	502
438	352	200 (4)

Frequency Grouping

3044 (6) 2209 (3) 1421 (7) 1025 (5) 761 (3) 466 (4) 154 (6)

Moments of Inertia (amu-A^2): 3.1 (1-D, σ = 3)

Table IV

Reactant: *tert*-Butoxide Anion

Frequencies (cm^{-1})		
2988 (2)	2973 (2)	2943
2918	2908	2876 (2)
1477 (2)	1469 (2)	1464
1450	1392	1373 (2)
1214 (2)	1140	1027
1013 (2)	921 (2)	915
746	456 (2)	418
348 (2)	270 (2)	

Internal Moments of Inertia (amu-A^2): 3.1 (1-D, σ = 3)

External Moments of Inertia: 112.0, 109.0, 107.0

Complex: Cleavage Transition State

Frequencies (cm^{-1})		
3161 (2)	3044	3018 (2)
2972 (2)	2920 (2)	1697
1444	1431	1426
1410	1398 (2)	1364 (2)
1216	1091	1066
905	872	787
607	527	484
385	200 (4)	109
105		

Frequency Grouping for Direct Counting Procedure

3019 (9) 1434 (9) 1122 (3) 853 (3) 494 (4) 200 (4) 107 (2)

Internal Moments of Inertia (amu-A^2): 3.1 (1-D, σ = 3)

External Moments of Inertia: 185.0, 170.0, 116.0

Several previously reported studies can be reinterpreted in light of our present study. The isotope effects and the model calculations reported here provide strong support for a general stepwise

(45) Simple cleavages of positive ions to form alkyl radicals, such as those discussed by McLafferty (ref 46) and others (ref 47 and 48) exhibit secondary isotope effects that are comparable to those observed in the pulsed CO_2 laser photolysis of *tert*-butoxide anion.

(46) McLafferty, F. W.; McAdoo, D. J.; Smith, J. S.; Kornfeld, R. *J. Am. Chem. Soc.* **1971**, *93*, 3720.

(47) Neeter, R.; Nibbering, N. M. M. *Org. Mass Spec.* **1973**, *7*, 1091. Broer, W. J.; Weringa, W. D. *Org. Mass Spec.* **1979**, *14*, 36.

(48) Jones, G.; McDonnell, L. P. *Org. Mass Spec.* **1975**, *10*, 1. Eadon, G.; Zawalski, R. *Org. Mass Spec.* **1977**, *12*, 599.

(49) Wendelboe, J. F.; Bowen, R. D.; Williams, D. H. *J. Am. Chem. Soc.* **1981**, *103*, 2333.

(50) Tumas, W.; Foster, R. F.; Brauman, J. I. *J. Am. Chem. Soc.* **1984**, *106*, 4053.

(51) All of the vibrational frequencies of acetone and its deuteriated analogues have been reported. Dellapiane, G.; Overend, J. *Spect. Acta* **1966**, *22*, 593. Shimanouchi, T. *Tables of Molecular Vibration Frequencies, NBS Ref. Data Series*; 1967. To a good approximation, there should be no difference between acetone and acetone radical anion except for the carbonyl stretching frequency.

mechanism for formal 1,2-elimination of alkanes from gas-phase ions.[10,29]

Finally, we note one additional intriguing feature of the decomposition of *tert*-butoxide anion. The proton-transfer reaction within the activated intermediate which comprises the second step of this multistep fragmentation is highly exothermic (ca. 40 kcal/mol). Although the nature of the partitioning of the excess energy into the products is not known, it is likely that the product acetone enolate ion will be vibrationally excited. Experiments designed to detect a red-shifted threshold in the optical electron photodetachment spectrum of the product enolate ion are in progress.

Acknowledgment. We are grateful to Dr. Charles M. Lieber and Dr. Paul B. Comita for helpful discussions and comments. This work was supported by the National Science Foundation and the donors of the Petroleum Research Fund, administered by the American Chemical Society. The CW CO_2 laser was constructed with assistance from the San Francisco Laser Center supported by the National Science Foundation under Grant NSF CHE79-1250. We thank the National Science Foundation for postdoctoral fellowship support for R.F.F. and for graduate fellowship support for W.T. and M.J.P. W.T. also gratefully acknowledges fellowship support from the Fannie and John Hertz Foundation.

Appendix 1. Calculation of Isotope Effects

The exact method for calculating the primary and secondary isotope effects from the observed product acetone enolate ion ratios in the decomposition of the deuteriated *tert*-butoxide ions depends on the operative reaction mechanism. Expressions for the secondary and primary isotope effects in terms of the product enolate ion abundances are presented in this appendix.

For a concerted process, the reaction path degeneracies for elimination of the three possible isotopically distinct methanes from a deuteriated alkoxide are all equal ($\sigma = 6$ for each reaction channel). Therefore, the isotope effects can be taken directly from the appropriate enolate ratios. Here, we use $[CX_3L]$ to denote the abundance of the enolate ion resulting from CX_3L elimination (X, L = H, D). Primed variables (′) designate the rate constants and ratios for the d_6 alkoxide **2**; unprimed variables refer to the d_3 ion **1**.

$$\text{primary effect} = [CX_3H]/[CX_3D] \quad (\mathbf{1};\ X = H,\ \mathbf{2};\ X = D)$$

$$\text{secondary effect} = [CH_3L]/[CD_3L] \quad (\mathbf{1};\ L = H,\ \mathbf{2};\ L = D)$$

For a stepwise mechanism with more than one branching point, such as the proposed mechanism involving initial cleavage to an ion–molecule complex and a subsequent hydrogen transfer reaction, the effects must be calculated differently because isotope effects and statistical factors appear in different steps. The scheme for this mechanism along with the expressions for the statistically corrected isotope effects is presented below for the d_3 and d_6 alkoxides where $k_1^{CX_3}$ refers to the microcanonical rate constant averaged over the appropriate energy distribution function for the loss of CX_3 in the first step, and k_2^{L} refers to the second step which involves transfer of the atom L. The process involving heterolytic cleavage is illustrated here; however, the equations are the same regardless of the nature of the cleavage in the first step. These

	secondary	primary
1	$\dfrac{k_1^{CH_3}}{k_1^{CD_3}} = \dfrac{[CH_3H]+[CH_3D]}{2[CD_3H]}$	$\dfrac{k_2^{H}}{k_2^{D}} = \dfrac{[CH_3H]}{[CH_3D]}$
2	$\dfrac{k_1^{CH_3'}}{k_1^{CD_3'}} = \dfrac{2[CH_3D]'}{[CD_3H]'+[CD_3D]'}$	$\dfrac{k_2^{H'}}{k_2^{D'}} = \dfrac{[CD_3H]'}{[CD_3D]'}$

equations were derived assuming irreversibility of the first step. The algebraic expressions incorporating reversible cleavage (i.e., k_{-1} as the reverse of k_1) are somewhat more complex; however, the deviation of the values for the isotope effects from those determined by using the above expressions would be minimal.[38] As the first step becomes reversible, the overall observable secondary kinetic isotope effect tends toward the value for the equilibrium isotope effect for the first step (i.e., $[k_1^{CH_3}/k_{-1}^{CH_3}]/[k_1^{CD_3}/k_{-1}^{CD_3}]$) which is greater than or equal to the kinetic isotope effect for the cleavage reaction. For highly endoergic cleavage reactions, the kinetic and equilibrium isotope effects are nearly equal, because the structure of the transition state for cleavage and the resulting intermediate are similar in structure (similar zero-point energies).[38] In other words, reversibility tends to maximize an intramolecular isotope effect in a bond cleavage reaction. Since the cleavage reaction for *tert*-butoxide ion is highly endoergic, the zero-point energy difference of the transition states in the first step (and thus the isotope effect) is already nearly maximized; the structure of this transition state is close to that of the intermediate (see Scheme III).

Appendix 2. Model Calculations

Intramolecular secondary isotope effects for the stepwise decomposition of *tert*-butoxide anion were calculated by using RRKM theory.[8,30] The microcanonical rate constant, $k(E)$, for a unimolecular reaction is given by eq 12 where h is Planck's constant, σ is the reaction path degeneracy, $N(E)$ is the density of internal rotational and vibrational states of the reactant at an internal energy E, and $G(E - E_0)$ is the sum of internal states for the transition state with a critical energy E_0. The intramolecular microcanonical kinetic isotope effect, $k(E)/k'(E)$, is simply the ratio of the state sums for the two isotopically distinct transition states (with equal reaction degeneracies) since the same reactant is involved. Primes (′) are used to denote the heavier isotope. In

$$k(E) = \sigma G(E - E_0)/hN(E) \quad (12)$$

$$k(E)/k'(E) = G(E - E_0)/G(E - E_0') \quad (13)$$

$$b(E) = k(E)/[k(E) + k'(E)] \quad (14)$$

the calculation of the secondary isotope effects we have defined a branching fraction, $b(E)$, which varies only between unity and zero. To calculate the ratio of the rate constants for loss of the CH_3 and CD_3 from 2-methyl-2-propoxide-*1,1,1-d*$_3$ anion (**1**), a model for the frequencies and structure of the transition state as well as an assessment of the critical energy differences for the two channels are required.

Transition State Model. The parameters for the transition state for loss of methyl radical or anion from *tert*-butoxide anion were chosen by modelling this reaction as a simple bond cleavage. The structure of this transition state was modeled as a complex of methyl radical and acetone radical anion (or of methyl anion and acetone). Such a model is justified by the large endothermicity of this cleavage reaction and the likelihood that the barrier is not in considerable excess of the thermodynamic one. In addition, this type of model has been successfully applied to a wide range of reactions of both neutral and ionic systems that only involve bond dissociation.[30] The majority of the frequencies for the transition state were taken from the reported values for methyl radical and acetone[23,24,51] (30 of the 36 internal degrees of vibrational freedom present in the reactant alkoxide ion). One of the remaining six vibrational degrees of freedom becomes the reaction coordinate in the transition state, and the other five become internal rotations in the intermediate ion–molecule complex: two two-dimensional rotors (one each for the methyl and acetone moieties) and a single one-dimensional rotor with a reduced moment of inertia. In transition states for bond dissociations[30] these rotations are usually considered to be hindered and can be treated as low-frequency vibrations (ca. 100–300 cm^{-1}). The 35 vibrational frequencies for each transition state were grouped into seven sets for the calculations by using direct counting procedures.[37]

Zero-Point Effects. The difference between the critical energies for the two isotopically distinct transition states is determined only by the difference in zero-point energies fixed by changes in the vibrational frequencies in the transition states. A maximum

$$E_0 - E_0' = h/2\sum(\nu_i - \nu_i') \quad (15)$$

zero-point energy difference of ca. 280 cm^{-1} (0.8 kcal/mol) is obtained with CH_3 loss being lower in energy. The major con-

tributors to this zero-point energy difference are the isotopically sensitive umbrella mode and two rocking modes of the methyl groups which are much larger in a covalently bound methyl (in acetone) than in the free methyl moiety.

Input Parameters. The frequencies used to model the transition states in the RRKM calculations of the secondary isotope effect for the stepwise mechanism are listed in Table III. Transition state A and B correspond to CD_3 and CH_3 cleavage, respectively. The input data for the calculation of the absolute rate constants for the first step of the stepwise mechanism (cleavage to the intermediate ion–molecule complex) are given in Table IV.

Registry No. *t*-BuO^-, 16331-65-0; D_2, 7782-39-0; CD_3I, 865-50-9; Me_2CO, 67-64-1; MeBr, 74-83-9; $(CD_3)_2CO$, 666-52-4; *t*-$BuOSiMe_3$, 13058-24-7; Me_3SiCl, 75-77-4; $Me_3SiNHAc$, 13435-12-6; $CD_3CMe_2OSiMe_3$, 105457-97-4; 2-methyl-2-propanol-*1,1,1*-d_3, 33500-15-1; 2-methyl-2-propanol-*1,1,1,3,3,3*-d_6, 53853-65-9.

The Mechanism of Directed Second Lithiations: Detection of Short Proton–Lithium Separations by ^6Li–^1H HOESY

Walter Bauer, Timothy Clark,* and Paul von Ragué Schleyer

Contribution from the Institut für Organische Chemie der Friedrich-Alexander-Universität, Erlangen-Nürnberg, D-8520 Erlangen, Federal Repulic of Germany. *Received July 3, 1986*

Abstract: Mechanistic details of the specific second metalation of 1-lithionaphthalene (**1**) at the 8-(peri) position, which should be typical of this important class of reactions, have been clarified by a combination of experimental (NMR) and theoretical (MNDO) methods. Complete structural assignments of the ^1H and ^{13}C NMR spectra for both *n*-butyllithium (BuLi) in THF-d_8 and **1** in C_6D_6 have been obtained from two-dimensional (2D) NMR experiments (COSY, C–H shift correlation). ^6Li–^1H HOESY (2D-heteronuclear Overhauser spectroscopy) exhibits cross peaks for $H(C_1)$ and $H(C_2)$ in the BuLi tetramer, indicating some of the Li–H distances to be unusually short. Applied to **1**, the same technique reveals a small distance between Li and $H(C_2)$. However, for a 1:1 mixture of methyllithium and **1**, ^6Li–^1H HOESY reveals a close contact between Li and $H(C_8)$ (periposition). MNDO calculations indicate that the 2-position of **1** dimer exhibits the shortest H···Li distance but that the 8-position in the mixed CH_3Li–**1** aggregate should be activated. This supports the proposed mechanism for the specific second metalation of **1** by BuLi, which involves reaction within a mixed cluster of **1** and the RLi metalation reagent.

The presence of lithium in a molecule often directs further metalation to a specific position.[1] For example, *n*-butyllithium (BuLi) converts 1-lithionaphthalene (**1**) to the 1,8-dilithio derivative (**2**). On the basis of semiempirical MO calculations, we have suggested that C—Li···H bridging in mixed alkyl/aryl lithium clusters may be responsible for specifically activating one C–H bond in the molecule.[1] We now report a combined NMR and MNDO investigation designed to elucidate the structures of the species found in alkyl/aryl lithium reaction mixtures in solution. These are often, but not always, related to crystal structures obtained by X-ray crystallography[2,3] but involve species for which crystalline samples cannot be obtained. We have applied ^1H–^1H shift correlation (correlated spectroscopy, COSY) and ^{13}C–^1H shift correlation spectroscopy[4] to assign completely the spectra of the lithium compounds investigated. The ^1H chemical shifts thus obtained form the basis for the application of two-dimensional heteronuclear Overhauser spectroscopy (HOESY)[5] (analogous to the homonuclear NOESY[6] experiment), using ^6Li and ^1H nuclei. This technique, which has never been applied to ^6Li nuclei before, allows the detection of close Li–H contacts. We have suggested such contacts to be responsible for C–H activation. The use of a high-field (9.4 T) spectrometer allows ^6Li–^1H HOESY experiments to be carried out with natural abundance samples. The results obtained are confirmed and extended by MNDO calculations.

NMR Results

We first describe the results of NMR investigations on *n*-butyllithium, which serve to illustrate the techniques employed, and then on 1-naphthyllithium (**1**).

***n*-Butyllithium (*n*-BuLi).** The nature of *n*-BuLi, the most important organolithium reagent, and the reactivity of its oligomers have been studied by ^1H NMR spectroscopy.[7] A dimer–tetramer equilibrium in tetrahydrofuran-d_8 (THF-d_8) solution at low temperatures was established both by ^1H[7] and by ^{13}C NMR,[8] and the kinetics were analyzed by NMR line shape analysis.[9] The full ^{13}C NMR assignment for a benzene-d_6 solution at room temperature (involving rapid interchange between aggregates on the NMR time scale) has been described.[10]

In 1.6 M *n*-BuLi in THF-d_8 at −96 °C, the dimer–tetramer equilibrium is shifted toward the tetramer. The one-dimensional ^1H NMR spectrum (Figure 1) shows the rotation around at least some of the C–C bonds to be slow on the NMR time scale. The magnetically nonequivalent pairs of α-, β- and γ-protons give rise

(1) This is the third paper in a series on regioselective metalations. (a) Part 1: Neugebauer, W.; Kos, A. J.; Schleyer, P. v. R. *J. Organomet. Chem.* **1982**, *228*, 107. (b) Part 2: Neugebauer, W.; Clark, T.; Schleyer, P. v. R. *Chem. Ber.* **1983**, *116*, 3283. Also see: Bauer, W.; Müller, G.; Pi, R.; Schleyer, P. v. R. *Angew. Chem.*, in press.

(2) Wardell, J. L. In *Comprehensive Organometallic Chemistry*; Wilkinson, G., Stone, F. G. A., Abel, E. W., Eds.; Pergamon: Oxford, 1982; Vol. 1, p 43ff.

(3) Setzer, W. N.; Schleyer, P. v. R. *Adv. Organomet. Chem.* **1985**, *24*, 353. Schleyer, P. v. R. *Pure Appl. Chem.* **1984**, *56*, 151.

(4) Bax, A. *Two Dimensional Nuclear Magnetic Resonance*; D. Reidel: Dordrecht (Holland), 1984. Günther, H. *Angew. Chem., Int. Ed. Engl.* **1983**, *22*, 350.

(5) Yu, C.; Levy, G. C. *J. Am. Chem. Soc.* **1984**, *106*, 6533.

(6) Jeener, J.; Meier, B. H.; Bachmann, P.; Ernst, R. R. *J. Chem. Phys.* **1979**, *71*, 4546. Meier, B. H.; Ernst, R. R. *J. Am. Chem. Soc.* **1979**, *101*, 6441.

(7) McGarrity, J. F.; Ogle, C. A. *J. Am. Chem. Soc.* **1985**, *107*, 1805. McGarrity, J. F.; Ogle, C. A.; Brich, Z.; Loosli, H.-R. *J. Am. Chem. Soc.* **1985**, *107*, 1810.

(8) Seebach, D.; Hässig, R.; Gabriel, J. *Helv. Chim. Acta* **1983**, *66*, 308.

(9) Heinzer, J.; Oth, J. F. M.; Seebach, D. *Helv. Chim. Acta.* **1985**, *68*, 1848.

(10) Bywater, S.; Lachance, P.; Worsfold, D. J. *J. Phys. Chem.* **1975**, *79*, 2148.

0002-7863/87/1509-0970$01.50/0